The two-phase model for calculating thermodynamic properties of liquids from molecular dynamics: Validation for the phase diagram of Lennard-Jones fluids

Shiang-Tai Lin, Mario Blanco, and William A. Goddard III[a)]
Materials and Process Simulation Center, Beckman Institute, 139-74 California Institute of Technology, Pasadena, California 91125

(Received 6 February 2003; accepted 12 September 2003)

We propose a general approach for determining the entropy and free energy of complex systems as a function of temperature and pressure. In this method the Fourier transform of the velocity autocorrelation function, obtained from a short (20 ps) molecular dynamics trajectory is used to obtain the vibrational density of states (DoS) which is then used to calculate the thermodynamic properties by applying quantum statistics assuming each mode is a harmonic oscillator. This approach is quite accurate for solids, but leads to significant errors for liquids where the DoS at zero frequency, $S(0)$, remains finite. We show that this problem can be resolved for liquids by using a two phase model consisting of a solid phase for which the DoS goes to zero smoothly at zero frequency, as in a Debye solid; and a gas phase (highly fluidic), described as a gas of hard spheres. The gas phase component has a DoS that decreases monotonically from $S(0)$ and can be characterized with two parameters: $S(0)$ and $3N^g$, the total number of gas phase modes [$3N^g \rightarrow 0$ for a solid and $3N^g \rightarrow 3(N-1)$ for temperatures and pressures for which the system is a gas]. To validate this two phase model for the thermodynamics of liquids, we applied it to pure Lennard-Jones systems for a range of reduced temperatures from 0.9 to 1.8 and reduced densities from 0.05 to 1.10. These conditions cover the gas, liquid, crystal, metastable, and unstable states in the phase diagram. Our results compare quite well with accurate Monte Carlo calculations of the phase diagram for classical Lennard-Jones particles throughout the entire phase diagram. Thus the two-phase thermodynamics approach provides an efficient means for extracting thermodynamic properties of liquids (and gases and solids). © *2003 American Institute of Physics.*
[DOI: 10.1063/1.1624057]

I. INTRODUCTION

Entropy and free energy as a function of temperature and pressure are essential in describing the phase diagram of liquids of materials. It would be most valuable to extract this information from atomistic classical and quantum simulations. However, the need for extensive sampling of the available energy states makes it a challenge to determine these quantities accurately. Techniques that extend the Widom particle insertion or thermodynamic integration methods to efficiently and accurately determine the phase equilibria of a wide variety of systems include the Gibbs ensemble, multiple histograms, configuration biased samplings.[1] In principle, these techniques provide rigorous thermodynamic quantities of complex systems; however, the large amount of sampling needed makes such methods impractical for many systems of interest. Thus, it is highly desirable to find ways to obtain fast and accurate estimates of the entropy and free energy from simple molecular dynamics simulations.

One possibility is to apply quantum statistics to the normal vibrational modes of a system, e.g., the Debye theory of crystals.[2] For crystals, the vibrational modes can be considered as harmonic and the thermodynamic properties can be expressed as integrals of functionals over the vibrational density of states. This method requires knowledge only of the vibrational density of state (DoS); however, the extension to fluids is nontrivial. Figure 1 shows the typical density of state distribution, $S(\upsilon)$, for a gas, a liquid, and a solid as a function of frequency υ. For a solid [Fig. 1(a)] the general form has $S(0)=0$ with $S(\upsilon)$ going through a maximum at finite υ, and then decaying for higher frequencies. For a gas [Fig. 1(b)], $S(0)>0$ and decays monotonically. The DoS of liquids [Fig. 1(c)] also has $S(0)>0$, and generally leads to a local minimum at low frequency and a solidlike maximum at higher frequency followed by decay for higher frequencies interspersed with broadened peaks due to local vibrations. As discussed below, the zero frequency intensity $S(0)$ corresponds to the diffusive modes of the system. Since the harmonic oscillator has infinite entropy at $\upsilon=0$, the direct application of quantum statistics to gases and liquids would result in an infinite entropy because of the nonzero value $S(0)$. Furthermore, the low frequency vibrations are usually quite anharmonic and the use of the simple harmonic approximation breaks down at this limit. These properties of fluids [nonzero $S(0)$ and anharmonicities] will be referred to as fluidic effects hereafter.

Despite these problems, the vibrational density of states has been used to study the thermodynamic properties of some important systems. Berens *et al.*[3] applied both quantum and classical statistics of a harmonic oscillator (HO) to the

a)Author to whom correspondence should be addressed. Electronic mail: wag@wag.caltech.edu

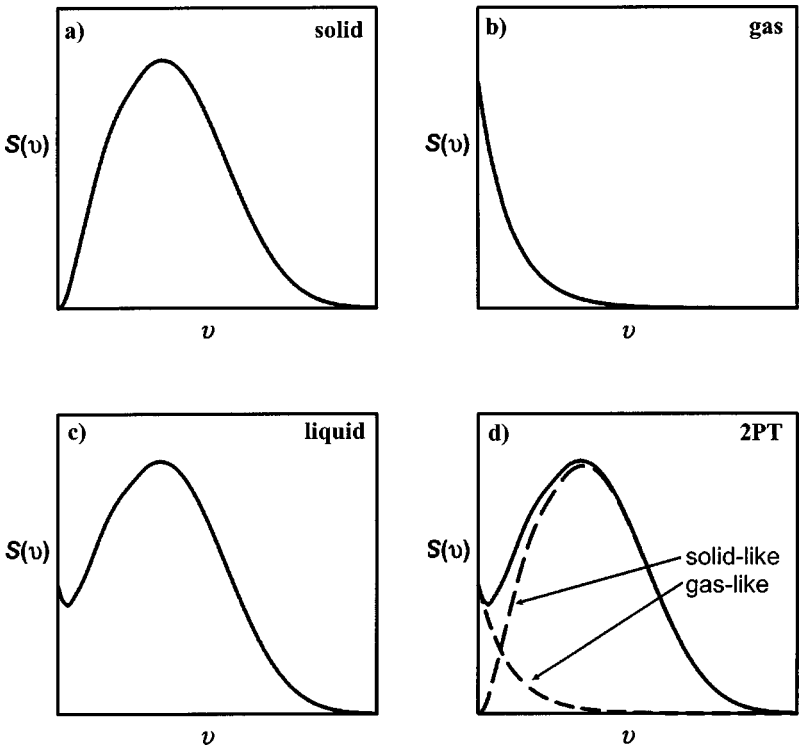

FIG. 1. Typical density of state distribution (DoS) of a solid (a), gas (b), and liquid (c). (d) shows that the liquid phase DoS can be a supposition of a gas and a solid DoS.

vibrational density of state (determined from the Fourier transform of the velocity autocorrelation function) and determined the quantum corrections to the thermodynamics of water. They showed that the method is useful because quantum effects are small at low frequencies where anharmonic effects are large, and are significant at high frequencies where anharmonicities are negligible.

Karplus and Kushick[4] proposed a quasiharmonic method that uses the covariance matrix of atomic position fluctuations to determine the vibrational frequencies, and argued that the *relative* configurational entropy differences of a flexible macromolecule in two different conformations can be determined from the logarithm of the ratio of the determinant of the covariance (Hessian) in the two conformations. Since anharmonic effects are not explicitly considered, the success of their method may largely be a result of cancellation of errors, due to anharmonicities, in the two conformations. More recently, Schlitter[5] proposed to apply a modified quantum statistical harmonic oscillator model to the quasiharmonic frequencies from the covariance matrix to obtain *absolute* entropies. Although the modified formula is an approximation to the exact quantum statistics of HO,[6] Schäfer and co-workers have used Schlitter's method to explain the entropic driving force in protein folding.[7,8] Schäfer *et al.*[7] performed limited tests of the Schlitter's method for the anharmonic effects and found 17% error in entropy for an ideal gas and only 5% error for Lennard-Jones (LJ) gases. They concluded that anharmonic effects are small in most cases. Andricioaei and Karplus[6] later re-examined the LJ calculation and found that the entropy obtained by Schäfer *et al.*[7] was not converged and the error increased with the simulation time. Since the fluidic effects (anharmonicity and diffusion) are not properly handled, we do not expect to obtain an accurate entropy value from Schlitter's method.

In this paper, we address this problem by proposing a two-phase model in which the DoS is decomposed into a gas phase component (described in terms of a hard sphere model) and a solid phase, whose density of states goes to zero at zero frequency. This is motivated by the observation that the shape of the DoS of a liquid is a simple supposition of that of a gas and a solid [Fig. 1(d)]. The gas component mostly contributes in the low frequency regime and contains all the fluidic effects, whereas the solid component, located at higher frequencies, has no fluidicity but can possess strong quantum effects. To test this two-phase thermodynamic (2PT) model, we calculated the thermodynamic properties of Lennard-Jones systems over a range of temperatures and pressures that includes gas, liquid, crystal, metastable, and unstable phases. We show that the standard one-phase model overestimates the entropy for dilute gases and underestimates the entropy for liquids due to fluidic effects. In 2PT, the gas phase component is characterized with two parameters, the fraction of the modes in the gas phase and $S(0)$, both of which are determined from the same molecular dynamics simulation. Applying the proper statistical weighting functions for each component leads to accurate thermodynamic properties. The time scale necessary for accurate thermodynamic properties is $\sim$20 ps (assuming that the system is equilibrated), making this a practical approach for complex systems. We find that 2PT leads to results in good agreement with Monte Carlo calculations for the thermodynamic properties of LJ fluids over a range of conditions including gas, liquid, solid, and metastable regions.

II. THEORY

A. The density of state function

The density of state (DoS) function $S(\upsilon)$ is defined as the distribution of vibrational normal modes of a system.[3] The number of modes, i.e., effective vibration intensity, of a system at some frequency υ is calculated as the sum of contributions from all atoms in the system,

$$S(\upsilon)=\frac{2}{kT}\sum_{j=1}^{N}\sum_{k=1}^{3} m_j s_j^k(\upsilon), \tag{1}$$

where m_j is the mass of atom j. The spectral density $s_j^k(\upsilon)$ of atom j in the kth coordinate ($k=x$, y, and z in the Cartesian coordinate) is determined from the square of the Fourier transform of the velocities as

$$s_j^k(\upsilon)=\lim_{\tau\to\infty}\frac{\left|\int_{-\tau}^{\tau} v_j^k(t)e^{-i2\pi\upsilon t}dt\right|^2}{\int_{-\tau}^{\tau}dt}$$

$$=\frac{|A_j^k(\upsilon)|^2}{\lim_{\tau\to\infty}\int_{-\tau}^{\tau}dt}=\lim_{\tau\to\infty}\frac{1}{2\tau}\left|\int_{-\tau}^{\tau} v_j^k(t)e^{-i2\pi\upsilon t}dt\right|^2, \tag{2}$$

where $v_j^k(t)$ is the kth velocity component of atom j at time t, and

$$A_j^k(\upsilon)=\lim_{\tau\to\infty}\int_{-\tau}^{\tau} v_j^k(t)e^{-i2\pi\upsilon t}dt. \tag{3}$$

The density of state function can also be obtained from the Fourier transform of the velocity autocorrelation function (VAC). The total velocity autocorrelation function $C(t)$ is defined as the mass weighted sum of the atom velocity autocorrelation functions

$$C(t)=\sum_{j=1}^{N}\sum_{k=1}^{3} m_j c_j^k(t), \tag{4}$$

where $c_j^k(t)$ is the velocity autocorrelation of atom j in the k direction

$$c_j^k(t)=\lim_{\tau\to\infty}\frac{\int_{-\tau}^{\tau} v_j^k(t'+t)v_j^k(t')dt'}{\int_{-\tau}^{\tau}dt'}$$

$$=\lim_{\tau\to\infty}\frac{1}{2\tau}\int_{-\tau}^{\tau} v_j^k(t'+t)v_j^k(t')dt'. \tag{5}$$

Applying the Wiener–Khintchine theorem,[2] the atomic spectrum density $s_j^k(\upsilon)$ is simply the Fourier transform of $c_j^k(t)$,

$$s_j^k(\upsilon)=\lim_{\tau\to\infty}\frac{1}{2\pi}\left|\int_{-\tau}^{\tau} v_j^k(t)e^{-i2\pi\upsilon t}dt\right|^2$$

$$=\lim_{\tau\to\infty}\frac{1}{2\tau}\int_{-\tau}^{\tau}\int_{-\tau}^{\tau} v_j^k(t)v_j^k(t+t')dt'e^{-i2\pi\upsilon t}dt$$

$$=\lim_{\tau\to\infty}\int_{-\tau}^{\tau} c_j^k(t)e^{-i2\pi\upsilon t}dt. \tag{6}$$

Therefore, $S(\upsilon)$ defined in Eq. (1) can also be obtained from the Fourier transform of $C(t)$,

$$S(\upsilon)=\frac{2}{KT}\sum_{j=1}^{N}\sum_{k=1}^{3} m_j s_j^k(\upsilon)$$

$$=\frac{2}{kT}\lim_{\tau\to\infty}\int_{-\tau}^{\tau}\sum_{j=1}^{N}\sum_{k=1}^{3} m_j c_j^k(t)e^{-i2\pi\upsilon t}dt$$

$$=\frac{2}{kT}\lim_{\tau\to\infty}\int_{-\tau}^{\tau} C(t)e^{-i2\pi\upsilon t}dt. \tag{7}$$

B. Properties of the density of state function

It is useful to outline the important properties of the density of state function, most of which have been previously discussed by Berens *et al.*[3] First of all, the value of $S(\upsilon)$ represents the density of normal modes at frequency υ,

$$S(\upsilon)=\sum_{i=1}^{3N}[\delta(\upsilon-\upsilon_i^{\mathrm{n}})+\delta(\upsilon+\upsilon_i^{\mathrm{n}})], \tag{8}$$

where υ_i^{n} are the normal mode frequencies of the system. Equation (8) can be shown to be true by substituting in Eqs. (4), (5), and (7) the normal mode velocities from the time derivative of the normal coordinates q_i, e.g., $q_i=A_i\sin(2\pi\upsilon_i^{\mathrm{n}}+\vartheta_i)$, with A_i and ϑ_i being the amplitude and phase of the ith degree of freedom.[3]

Furthermore, the integration of $S(\upsilon)$ over positive frequencies gives the total number of degrees of freedom ($3N$) of the system,

$$\int_0^{\infty} S(\upsilon)d\upsilon=\frac{1}{2}\int_{-\infty}^{\infty} S(\upsilon)d\upsilon$$

$$=\frac{1}{kT}\sum_{j=1}^{N}\sum_{k=1}^{3} m_j\int_{-\infty}^{\infty} s_j^k(\upsilon)d\upsilon$$

$$=\frac{1}{kT}\sum_{j=1}^{N}\sum_{k=1}^{3} m_j\overline{v_j^k(t)^2}$$

$$=\frac{1}{kT}\sum_{j=1}^{N}\sum_{k=1}^{3} kT=3N, \tag{9}$$

where the Parseval's theorem $[\int_{-\infty}^{\infty}|A_j^k(\upsilon)|^2d\upsilon=\int_{-\infty}^{\infty}v_j^k(t)^2dt]$ is used to relate the integration of $s_j^k(\upsilon)$ to the average of the square of the velocity,

$$\int_{-\infty}^{\infty} s_j^k(\upsilon)d\upsilon=\lim_{\tau\to\infty}\frac{1}{2\tau}\int_{-\tau}^{\tau}|A_j^k(\upsilon)|^2d\upsilon$$

$$=\lim_{\tau\to\infty}\frac{1}{2\tau}\int_{-\infty}^{\infty} v_j^k(t)^2dt=\overline{v_j^k(t)^2}. \tag{10}$$

The last equality in Eq. (10) is a result of the equipartition theorem in the classical limit, i.e., $m_j\overline{v_j^k(t)^2}=kT$.

The density of states at zero frequency $S(0)$ is related to the self-diffusion coefficient D in pure fluids. The diffusion coefficient is related to the velocity autocorrelation function as[2]

$$D=\frac{1}{3}\int_0^\infty c(t)dt=\frac{1}{6}\int_{-\infty}^\infty c(t)dt=\frac{1}{6mN}\int_{-\infty}^\infty C(t)dt, \tag{11}$$

where N is the number of particles and m is the mass of the particles. By setting the frequency ν to zero in Eq. (7) we have

$$S(0)=\frac{2}{kT}\int_{-\infty}^\infty C(t)dt=\frac{12mND}{kT}. \tag{12}$$

Finally, any properties derived from $S(\nu)$ can be easily broken down to atomic contributions since the total $S(\nu)$ is determined from the sum of the atomic spectral densities [Eq. (1)]. For example, one can study the diffusion of each individual atom or for a subcollection of atoms in the system. This property of $S(\nu)$ also provides a natural way of partitioning the thermodynamic properties, such as entropy (detailed in Secs. II C and II D) into atom or atomic group contributions, an intriguing prospect for molecular analysis of significantly higher detail than any prior efforts.

C. Thermodynamic properties and quantum corrections from the density of state function: The one-phase model

Assuming that all the vibrations are independent (uncorrelated) harmonic motions, the partition function Q of the system can be calculated from the partition function $q_{\mathrm{HO}}(\nu)$ of a harmonic oscillator as the following:

$$\ln Q=\int_0^\infty d\nu S(\nu)\ln q_{\mathrm{HO}}(\nu). \tag{13}$$

The energy E, entropy S, and Helmholtz free energy A of the system can then be determined as

$$E=V_0+T\beta^{-1}\left(\frac{\partial \ln Q}{\partial T}\right)_{N,V}=V_0+\beta^{-1}\int_0^\infty d\nu S(\nu)W_E(\nu), \tag{14a}$$

$$S=k\ln Q+\beta^{-1}\left(\frac{\partial \ln Q}{\partial T}\right)_{N,V}=k\int_0^\infty d\nu S(\nu)W_s(\nu), \tag{14b}$$

$$A=V_0-\beta^{-1}\ln Q=V_0+\beta^{-1}\int_0^\infty d\nu S(\nu)W_A(\nu). \tag{14c}$$

Substituting in these equations the quantum harmonic partition function

$$q^Q_{\mathrm{HO}}(\nu)=\frac{\exp(-\beta h\nu/2)}{1-\exp(-\beta h\nu/2)},$$

gives the quantum weighting functions,

$$W^Q_E(\nu)=\frac{\beta h\nu}{2}+\frac{\beta h\nu}{\exp(\beta h\nu)-1}, \tag{15a}$$

$$W^Q_S(\nu)=\frac{\beta h\nu}{\exp(\beta h\nu)-1}-\ln[1-\exp(-\beta h\nu)], \tag{15b}$$

$$W^Q_A(\nu)=\ln\frac{1-\exp(\beta h\nu)}{\exp(-\beta h\nu/2)}, \tag{15c}$$

where $\beta=1/kT$ and h is the Planck's constant. These weighting functions constitute the quantum-corrected one-phase thermodynamic model, 1PT(Q).

If instead we use a classical harmonic oscillator with $q^C_{\mathrm{HO}}(\nu)=1/\beta h\nu$, the weighting functions would take the following form:

$$W^C_E(\nu)=1, \tag{16a}$$

$$W^C_S(\nu)=1-\ln(\beta h\nu), \tag{16b}$$

$$W^C_A(\nu)=\ln(\beta h\nu). \tag{16c}$$

The use of these classical weighting functions in Eq. (14) gives the classical one-phase thermodynamic model, 1PT(C).

The reference energy V_0 [in Eqs. (14a) and (14c)] is the potential energy of the system when all the ''oscillators'' are at standing still. This energy is determined by equating the total energy E^{MD} from a MD simulation to the energy E^C of a set of classical harmonic oscillators [Eqs. (14a) and (16a)],

$$V_0=E^{\mathrm{MD}}-\beta^{-1}\int_0^\infty d\nu S(\nu)W^C_E(\nu)=E^{\mathrm{MD}}-\beta^{-1}3N. \tag{17}$$

The quantum effects (or quantum corrections) of a system can be determined from the differences between the quantum and classical properties, i.e.,

$$\Delta E^{\mathrm{QC}}=\beta^{-1}\int_0^\infty d\nu S(\nu)[W^Q_E(\nu)-W^C_E(\nu)], \tag{18a}$$

$$\Delta S^{\mathrm{QC}}=k\int_0^\infty d\nu S(\nu)[W^Q_S(\nu)-W^C_S(\nu)], \tag{18b}$$

$$\Delta A^{\mathrm{QC}}=\beta^{-1}\int_0^\infty d\nu S(\nu)[W^Q_A(\nu)-W^C_A(\nu)]. \tag{18c}$$

Therefore, the quantum effects can be completely determined for a given density of state distribution. The quantum corrections are zero at zero frequency and increase with increasing frequency[3] making them most important for system containing high frequency vibrations.

D. Density of states decomposition for the correction of fluidicity effects: The two-phase model

The harmonic approximation described above has been widely used in the study of thermodynamic properties of crystals because the harmonic assumption is reasonable in the solid phase. However, a direct extension to amorphous liquids and gases may be inappropriate since the entropy is dominated by low frequency modes where the effects of fluidicity are important. In particular, the entropy of a harmonic oscillator has a singularity (positive infinity) at zero frequency, which corresponds to the diffusion mode in fluids [Eq. (12)].

To resolve this problem, we propose a **Two-Phase Thermodynamic (2PT) model** in which the density of state $S(\nu)$ of the system with $3N$ degrees of freedom are partitioned into a gas and a solid like component

$$S(\nu)=S^g(\nu)+S^s(\nu), \tag{19}$$

where **the gaslike** diffusive component $S^g(\nu)$ corresponds to $3N^g=3fN$ degrees of freedom with f being the gas fraction and the remainder, $S^s(\nu)$, describes a **solidlike** component (non-diffusive) in which $S(0)=0$ (that is no diffusion). Thus there are $3N^s=3N-3N^g=3N(1-f)$ ''solidlike'' degrees of freedom. The thermodynamic properties P of the system are determined from weighting the individual density of state (DoS) component with proper functions

$$P=\int_0^\infty d\nu S^s(\nu)W_P^{\mathrm{HO}}(\nu)+\int_0^\infty d\nu S^g(\nu)W_P^g(\nu), \tag{20}$$

where $W_P^{\mathrm{HO}}(\nu)$ is the weighting function of a harmonic oscillator [Eq. (14) or (15)] and $W_P^g(\nu)$ is the weighting function corresponding to the choice of the gas component.

The 2PT model is uniquely specified by the form of $S^g(\nu)$, which by subtracting determines the form of $S^s(\nu)$. We find that a particularly suitable form for $S^g(\nu)$ is to describe the gaslike component as a hard sphere fluid. The velocity autocorrelation function $c^{\mathrm{HS}}(t)$ of a hard sphere gas decays exponentially[2]

$$c^{\mathrm{HS}}(t)=c^{\mathrm{HS}}(0)\exp(-\alpha t)=\frac{3kT}{m}\exp(-\alpha t), \tag{21}$$

where α is the Enskog friction constant related to the collisions between hard spheres. The DoS distribution is derived from the Fourier cosine transform of Eq. (21),

$$\begin{aligned}S^{\mathrm{HS}}(\nu)&=\frac{4}{kT}\int_0^\infty\sum_{j=1}^{N^g}\sum_{k=1}^{3}m_jc_j^k(t)\cos(2\pi\nu t)dt\\&=\frac{4}{kT}\int_0^\infty 3N^gkT\exp(-\alpha t)\cos(2\pi\nu t)dt\\&=\frac{12N^g\alpha}{\alpha^2+4\pi^2\nu^2},\end{aligned} \tag{22}$$

where $N^g=fN$ is the number of effective hard sphere particles in the system and f is the fraction of hard sphere component in the overall system. This fraction factor is a measure of the ''fluidicity'' of the system and should depend on both the temperature and density. Using the zero frequency value, i.e.,

$$S^{\mathrm{HS}}(0)=s_0=\frac{12fN}{\alpha}, \tag{23}$$

Eq. (22) can be rewritten as

$$S^g(\nu)=S^{\mathrm{HS}}(\nu)=\frac{s_0}{1+\left[\dfrac{\pi s_0\nu}{6fN}\right]^2}. \tag{24}$$

Therefore, **the DoS for the gas component is completely determined with two parameters**: s_0 **and** f. It is straightforward to determine s_0 since it is just the zero frequency DoS value for the total system $S(0)$. This guarantees that the solid component has no contribution to the diffusivity,

$$s_0=S^{\mathrm{HS}}(0)=S(0),\quad S^s(0)=0. \tag{25}$$

The only remaining question in defining 2PT theory is how to define the exact value of ''fluidicity'' factor f that determines the conceptual partition of the whole system between solid and gas components. We want f to satisfy two limiting conditions:

(1) In the high temperature and/or low density limit, the system behaves like hard spheres, therefore $f=1$, i.e., no solid component.
(2) In the high density limit where the system is a solid, we expect $f=0$, i.e., no gas component.

Thus we propose to define f as proportional to the diffusivity, which automatically satisfies the two above conditions. Thus we find it convenient to write

$$f=\frac{D(T,\rho)}{D_0^{\mathrm{HS}}(T,\rho;\sigma^{\mathrm{HS}})}, \tag{26}$$

where D is the self-diffusivity of the system determined from Eq. (12), and D_0^{HS} is the hard sphere diffusivity determined in the zero pressure limit (the Chapman–Enskog result)[2]

$$D_0^{\mathrm{HS}}(T,\rho;\sigma^{\mathrm{HS}})=\frac{3}{8}\frac{1}{\rho{\sigma^{\mathrm{HS}}}^2}\left(\frac{kT}{\pi m}\right)^{1/2}. \tag{27}$$

Tying our theory to hard sphere theory might seem limiting, but we show below that all parameters can be fully derived from the actual interatomic potentials describing the real atom of our system.

From Eq. (27) to completely determine f, we need only define the hard sphere diameter σ^{HS}. We do this by requiring the diffusivity of the gas component (at temperature T and density $f\rho$) to agree with that predicted by the Enskog theory,[2] which we believe gives the best transport properties for dense hard sphere fluids. The diffusivity of the gas component is determined from the VAC defined in Eq. (21),

$$D^{\mathrm{HS}}(T,f\rho)=\frac{1}{3}\int_0^\infty c^{\mathrm{HS}}(t)dt=\frac{kT}{m\alpha}=\frac{kTs_0}{12mfN}, \tag{28}$$

where Eq. (23) is used for α. The Enskog theory predicts the deviation of diffusivity for a dense hard sphere fluid from its zero pressure limit as

$$D^{\mathrm{HS}}(T,f\rho)=D_0^{\mathrm{HS}}(T,f\rho;\sigma^{\mathrm{HS}})\frac{4fy}{z(fy)-1}, \tag{29}$$

where z is the compressibility, which can be obtained from the accurate Carnahan–Starling equation of state[9] for hard spheres

$$z(y)=\frac{1+y+y^2-y^3}{(1-y)^3} \tag{30}$$

and y is the hard sphere packing fraction defined as $y=(\pi/6)\rho{\sigma^{\mathrm{HS}}}^3$. For a given value of f, Eqs. (28) and (29) can be used to solve for y, and thus σ^{HS}. However, since f in Eq. (26) is also a function of σ^{HS}, Eqs. (26), (28), and (29) must be solved simultaneously for both f and σ^{HS}.

We use the following procedure to solve for f. First we combine Eqs. (12), (23), and (28), to obtain $D^{\mathrm{HS}}(T,f\rho)=D(T,\rho)/f$. That is, the diffusivity of the gas component is $1/f$ times larger than the real system. Further, according to Eq. (27) we know that in the zero pressure limit

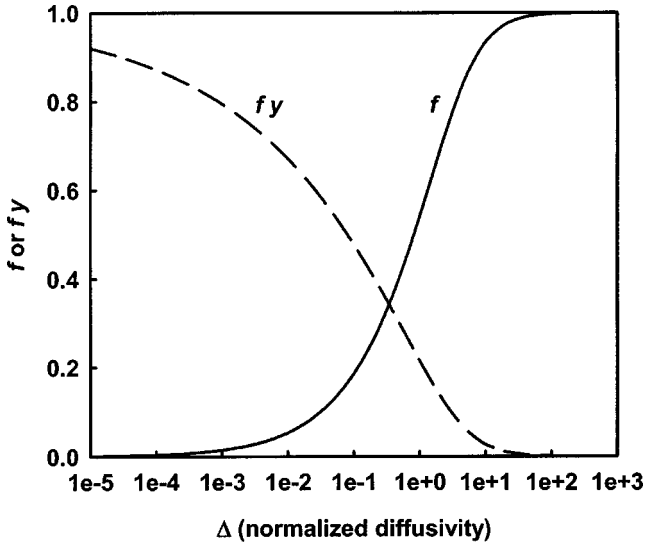

FIG. 2. Dependence of the fluidicity factory f and the packing fraction fy for the gas component on normalized diffusivity Δ [defined in Eq. (33)].

$D_0^{\mathrm{HS}}(T,f\rho)=D_0^{\mathrm{HS}}(T,\rho)/f$. Using these two identities and Eqs. (26), (29), and (30), we obtain a cubic equation for f in terms of y,

$$2y^3f^3-(y+6y^2)f^2+(2+6y)f-2=0. \tag{31}$$

Thus Eq. (31), which is system independent **determines the fluidicity f solely from the hard sphere packing fraction y for any system**. Equation (31) leads immediately to $f\to 1$ (no solid component) as $y\to 0$, $f\to 0$ (no gas component) as $y\to\infty$, and f decreases monotonically with increasing y. Another useful relationship is obtained by substituting Eq. (27) in Eq. (26) and rewriting the resultant equation in terms of y,

$$f=\Delta(T,\rho,m,s_0)y^{2/3}, \tag{32}$$

where the normalized diffusivity constant Δ is unitless and is a function of material properties

$$\Delta(T,\rho,m,s_0)=\frac{2s_0}{9N}\left(\frac{\pi kT}{m}\right)^{1/2}\rho^{1/3}\left(\frac{6}{\pi}\right)^{2/3}. \tag{33}$$

The Δ is proportional to the system diffusivity, which underlies many transport properties of the system. It includes effects of temperature, density, and different material characteristics (mass and diffusivity). Substituting Eq. (32) into Eq. (31), we obtain **a universal expression for f in terms of Δ**,

$$2\Delta^{-9/2}f^{15/2}-6\Delta^{-3}f^5-\Delta^{-3/2}y^{7/2}+6\Delta^{-3/2}f^{5/2}+2\,f-2=0. \tag{34}$$

Figure 2 shows the fluidicity factor f (solid curve) as a function of the normalized diffusivity Δ, where we see that $f\to 0$ as $\Delta\to 0$ and $f\to 1$ as $\Delta\to\infty$. Thus for a given value of Δ, Eq. (34) gives a unique value of f within 0 and 1. Figure 2 also shows the changes of the hard sphere packing fraction fy of the gas component (dotted curve) as a function of Δ. For large Δ (high temperature, low density, or highly diffusive) fy approaches 0, indicating that the whole system can be represented as a dilute gas. At small Δ values (low temperature, high density, or nondiffusive) fy approaches 1, which means that small fraction of the hard sphere gas component is very dense. **Therefore the normalized diffusivity Δ, which contains only the state condition (T,V,N) and the result from MD simulations (s_0), uniquely determines the fluidicity factor f of a system and is the key parameter that determines the gas–solid partition**.

To complete the 2PT model, we need to determine the weighting functions for the gas phase component (hard sphere diffusive fluid)

$$W_E^g(\upsilon)=W_E^{\mathrm{HS}}(\upsilon)=0.5, \tag{35a}$$

$$W_S^g(\upsilon)=W_S^{\mathrm{HS}}(\upsilon)=\frac{1}{3}\frac{S^{\mathrm{HS}}}{k}, \tag{35b}$$

$$W_A^g(\upsilon)=W_A^{\mathrm{HS}}(\upsilon)=W_E^{\mathrm{HS}}(\upsilon)-W_S^{\mathrm{HS}}(\upsilon). \tag{35c}$$

The excess entropy for a hard sphere fluid is determined from the packing fraction y as expressed by the Carnahan–Starling equation of state,[9] which in our model becomes

$$\frac{S^{\mathrm{HS}}}{k}-\frac{S^{\mathrm{IG}}}{k}=\ln[z(fy)]+\frac{fy(3fy-4)}{(1-fy)^2}, \tag{36}$$

where S^{IG} is the ideal gas contribution calculated at the same temperature and density. Finally the reference energy from Eq. (17) is modified as

$$V_0=E^{\mathrm{MD}}-\beta^{-1}\int_0^\infty d\upsilon[S^s(\upsilon)W_E^{\mathrm{HS}}(\upsilon)+S^g(\upsilon)W_E^g(\upsilon)]$$
$$=E^{\mathrm{MD}}-\beta^{-1}3N(1-0.5f), \tag{37}$$

where we used Eq. (35a). The simplicity of the above expressions arises from the frequency independence of the weighting functions for hard spheres. This allows us to obtain analytic expressions for the various quantities, showing the advantage of our definition of the gas phase as a hard sphere system.

Quantum effects in 2PT are included through the use of proper weighting function for the solid component in Eq. (20). Using classical statistics of a harmonic oscillator [Eq. (16)] for $W_P^{\mathrm{HO}}(\upsilon)$ leads to classical thermodynamic properties, the 2PT(C) model, whereas quantum statistics [Eq. (15)] gives the quantum-corrected properties, 2PT(Q). We show later that quantum effects are small for LJ systems ($<4\%$) but could be important for more complex molecular systems such as hydrocarbons and DNA.

In this paper, we develop and validate the approach for decomposing the DoS for pure Lennard-Jones fluids. Later work will extend the 2PT to mixtures and polyatomic systems.

III. COMPUTATIONAL DETAILS

The thermodynamic properties of Lennard-Jones (LJ) gas, liquid, and solid are used to examine the two-phase thermodynamic (2PT) model described in Sec. II D. The interaction potential V between two LJ particles is described through the standard LJ-12-6 equation

$$V=4\varepsilon\left[\left(\frac{\sigma}{r}\right)^{12}-\left(\frac{\sigma}{r}\right)^{6}\right], \tag{38}$$

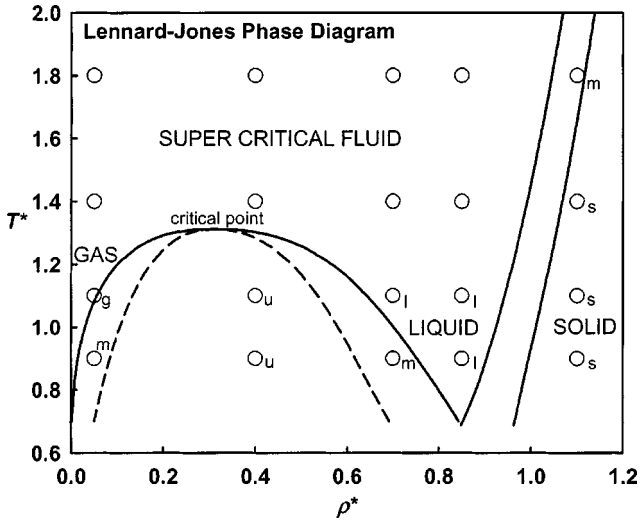

FIG. 3. Phase diagram of Lennard-Jones systems. The open circles represent the states studied in this work. The solid curves indicate the phase boundary (bimodal lines) and the dashed curves are the stability limits (spinodal lines) for liquid–gas equilibrium. Labels are added next to the open circles to help identify the thermodynamic state of each point (*s* for solid, *l* for liquid, *g* for gas, *m* for metastable, and *u* for unstable). For clarity, points in the supercritical regime are not labeled.

where r is the separation distance between two particles, and ε and σ are two parameters characterizing the strength of interaction and the size of the LJ particles. In this work, the parameters of argon ($\varepsilon = 0.238$ kcal/mol, $\sigma = 3.405$ Å^3, and mass $m = 39.948$ g/mol) are used in the actual MD simulations. To remain general the results are then presented in reduced units: density $\rho^* = \rho\sigma^3$, temperature $T^* = kT/\varepsilon$, pressure $P^* = P\sigma^3/\varepsilon$, energy $E^* = E/\varepsilon$, entropy $S^* = S/k$, Helmholtz free energy $A^* = A/\varepsilon$, Gibbs free energy $G^* = G/\varepsilon$, and diffusivity $D^* = D(m/\varepsilon)^{1/2}/\sigma$).

We consider a range of 5 densities and 4 temperatures (Fig. 3) including:

(1) 3 stable solid phases;
(2) 3 stable liquid phases;
(3) 1 stable gas phase;
(4) 8 supercritical fluid phases;
(5) 1 metastable solid phase;
(6) 1 metastable liquid phase;
(7) 1 metastable gas phase;
(8) 2 unstable fluid phases;

for a total of 20 state points to cover the phase diagram. CERIUS2 (Ref. 10) was used for all MD simulations. Constant volume, temperature, and number of particle (NVT) simulations are performed at each state point. Table I lists the details of the MD runs which ranged from a total of 160 ps (solids) to 640 ps (gas). [We will show later (Table IV) that it would have been possible to achieve similar accuracy with MD runs (after equilibration) of only 20 ps (gas) to 5 ps (solid and liquid).] Long-range interactions are included using the Ewald sum method (Accuracy Bounded Convergence[11] with accuracy parameter 0.001) and the Nosé–Hoover thermostat (time constant of 0.05 ps) is used to control the temperature.

TABLE I. Simulation conditions for systems studied in this work.

ρ^*	T^*	N	Equilibration steps	Sampling steps	Step size (fs)
0.05	0.9, 1.1,	512	10 000	80 000	8
0.40	1.4, 1.8	512	10 000	20 000	8
0.70		512	10 000	20 000	8
0.85		512	10 000	20 000	8
1.10		500[a]	10 000	40 000	4

[a]Face centered cubic lattice is used.

The simulation results are analyzed by calculating the velocity autocorrelation function and its Fourier transform to obtain the density of state distribution function $S(\upsilon)$. The zero frequency value $S(0)$ leads to self-diffusion coefficient D via Eq. (12). To determine thermodynamic properties using the 2PT model, the constant Δ is first calculated from Eq. (33) [where $s_0 = S(0)$] with the results for the 20 state points studied here listed in Table II. The fluidicity factor f is then solved from Eq. (34) (using Newton's method, results listed in Table II). Having $S(0)$ and f, the DoS of gas component $S^g(\upsilon)$ is completely determined [Eq. (24)]. The solid component $S^s(\upsilon)$ is obtained by subtracting $S^g(\upsilon)$ from the $S(\upsilon)$ of the real system. The thermodynamic properties are then determined from Eq. (20) with the gas and harmonic weighting functions given in Eqs. (15), (16), and (35).

IV. RESULTS AND DISCUSSIONS

A. Pressure, energy, and quantum effects

The pressure and energy for Lennard-Jones systems from our MD simulations are compared to the literature[12,13] equation of state (EOS) predictions in Table III and Fig. 4. For the fluid phase, the modified Benedict–Webb–Rubin (MBWR) EOS developed by Johnson *et al.*[12] is used while

TABLE II. The normalized diffusivity Δ calculated from Eq. (33) and the "fluidicity" fraction factor f determined from Eq. (34) for the 20 state points studied in this work.

	Δ T^*			
ρ^*	1.8	1.4	1.1	0.9
0.05	10.125	8.612	7.812	6.399[b]
0.40	2.024	1.886	1.653[a]	0.973[a]
0.70	0.964	0.781	0.703	0.667[b]
0.85	0.529	0.428	0.378	0.307
1.10	1.23×10^{-3}[b]	1.09×10^{-3}	8.05×10^{-4}	7.52×10^{-4}
	f T^*			
ρ^*	1.8	1.4	1.1	0.9
0.05	0.936	0.921	0.911	0.889[b]
0.40	0.690	0.675	0.647[a]	0.535[a]
0.70	0.534	0.491	0.470	0.460[b]
0.85	0.417	0.379	0.358	0.326
1.10	0.0163[b]	0.0152	0.0128	0.0123

[a]Unstable states.
[b]Metastable states.

TABLE III. Comparison of properties of Lennard-Jones systems calculated from different methods.

		Pressure P^*			
		T^*			
ρ^*	Method[a]	1.8	1.4	1.1	0.9
0.05	MD	0.082±0.004	0.060±0.004	0.042±0.004	0.029±0.004
	MBWR EOS	0.083	0.061	0.043	0.031
0.40	MD	0.537±0.098	0.195±0.084	−0.034±0.080	−0.082±0.085
	MBWR EOS	0.541	0.205	−0.038	−0.181
0.70	MD	2.457±0.244	1.279±0.201	0.343±0.174	−0.324±0.151
	MBWR EOS	2.482	1.291	0.345	−0.315
0.85	MD	6.024±0.334	4.095±0.301	2.500±0.234	1.363±0.201
	MBWR EOS	6.050	4.100	2.521	1.372
1.10	MD	15.989±0.490	12.742±0.393	10.287±0.316	8.624±0.256
	van der Hoef EOS	16.005	12.755	10.292	8.627
		Energy E^*			
		T^*			
ρ^*	Method[a]	1.8	1.4	1.1	0.9
0.05	2PT(Q)	2.338	1.702	1.186	0.768
	MD	2.338±0.035	1.702±0.024	1.185±0.027	0.766±0.052
	MBWR EOS	2.351	1.715	1.213	0.847
0.40	2PT(Q)	0.111	−0.652	−1.429	−2.639
	MD	0.105±0.052	−0.660±0.050	−1.442±0.080	−2.664±0.072
	MBWR EOS	0.101	−0.656	−1.324	−1.928
0.70	2PT(Q)	−1.698	−2.522	−3.153	−3.583
	MD	−1.719±0.068	−2.546±0.053	−3.181±0.042	−3.615±0.034
	MBWR EOS	−1.717	−2.544	−3.169	−3.608
0.85	2PT(Q)	−2.358	−3.297	−4.026	−4.520
	MD	−2.395±0.102	−3.340±0.078	−4.075±0.050	−4.576±0.041
	MBWR EOS	−2.402	−3.340	−4.051	−4.570
1.10	2PT(Q)	−3.420	−4.519	−5.338	−5.880
	MD	−3.508±0.129	−4.621±0.088	−5.456±0.064	−6.016±0.047
	van der Hoef EOS	−3.945	−4.611	−5.449	−6.010
		Entropy S^*			
		T^*			
ρ^*	Method[a]	1.8	1.4	1.1	0.9
0.05	1PT(Q)	18.136	17.267	16.419	15.155
	2PT(Q)	14.167	13.748	13.205	12.730
	2PT(C)	14.167	13.748	13.204	12.729
	MBWR EOS	14.071	13.671	13.267	12.900
0.40	1PT(Q)	11.685	10.979	10.033	8.372
	2PT(Q)	11.303	10.739	10.021	8.882
	2PT(C)	11.301	10.736	10.016	8.868
	MBWR EOS	11.138	10.662	10.122	9.513
0.70	1PT(Q)	9.191	8.576	7.972	7.465
	2PT(Q)	9.697	9.168	8.620	8.145
	2PT(C)	9.691	9.159	8.607	8.127
	MBWR EOS	9.510	8.990	8.487	8.046
0.85	1PT(Q)	8.034	7.378	6.741	6.215
	2PT(Q)	8.776	8.159	7.548	7.019
	2PT(C)	8.766	8.144	7.526	6.988
	MBWR EOS	8.582	7.992	7.420	6.899
1.10	1PT(Q)	6.090	5.435	4.801	4.282
	2PT(Q)	6.174	5.512	4.865	4.344
	2PT(C)	6.150	5.476	4.812	4.269
	van der Hoef EOS	6.226	5.525	4.851	4.288
		Helmholtz free energy A^*			
		T^*			
ρ^*	Method[a]	1.8	1.4	1.1	0.9
0.05	1PT(Q)	−30.300	−22.473	−16.871	−12.924
	2PT(Q)	−23.162	−17.544	−13.338	−10.689
	2PT(C)	−23.162	−17.544	−13.339	−10.690
	MBWR EOS	−22.977	−22.977	−13.381	−10.762

TABLE III. (*Continued*.)

0.40	1PT(Q)	−20.907	−16.008	−12.450	−10.156
	2PT(Q)	−20.232	−15.681	−12.448	−10.628
	2PT(C)	−20.235	−15.685	−12.455	−10.641
	MBWR EOS	−19.948	−19.948	−12.458	−10.489
0.70	1PT(Q)	−18.211	−14.502	−11.900	−10.280
	2PT(Q)	−19.136	−15.346	−12.628	−10.909
	2PT(C)	−19.146	−15.358	−12.642	−10.924
	MBWR EOS	−18.834	−18.834	−12.505	−10.850
0.85	1PT(Q)	−16.777	−13.593	−11.413	−10.088
	2PT(Q)	−18.129	−14.704	−12.319	−10.831
	2PT(C)	−18.148	−14.725	−12.344	−10.858
	MBWR EOS	−17.849	−17.849	−12.214	−10.779
1.10	1PT(Q)	−14.369	−12.118	−10.610	−9.727
	2PT(Q)	−14.526	−12.232	−10.687	−9.788
	2PT(C)	−14.570	−12.283	−10.746	−9.856
	van der Hoef EOS	−14.702	−14.702	−10.785	−9.869

Gibbs free energy G^*

		T^*			
ρ^*	Method[a]	1.8	1.4	1.1	0.9
0.05	1PT(Q)	−28.656	−21.286	−16.030	−12.356
	2PT(Q)	−21.522	−16.351	−12.495	−10.102
	2PT(C)	−21.522	−16.351	−12.496	−10.103
	MBWR EOS	−21.318	−16.215	−12.518	−10.142
0.40	1PT(Q)	−19.584	−15.521	−12.537	−10.361
	2PT(Q)	−18.889	−15.195	−12.535	−10.834
	2PT(C)	−18.892	−15.199	−12.541	−10.847
	MBWR EOS	−18.595	−15.070	−12.553	−10.941
70	1PT(Q)	−14.701	−12.675	−11.410	−10.743
	2PT(Q)	−15.626	−13.519	−12.138	−11.371
	2PT(C)	−15.637	−13.531	−12.152	−11.387
	MBWR EOS	−15.288	−13.286	−12.012	−11.299
0.85	1PT(Q)	−9.690	−8.776	−8.472	−8.484
	2PT(Q)	−11.042	−9.887	−9.378	−9.227
	2PT(C)	−11.061	−9.908	−9.403	−9.255
	MBWR EOS	−10.732	−9.706	−9.248	−9.165
1.10	1PT(Q)	0.167	−0.534	−1.258	−1.887
	2PT(Q)	0.009	−0.648	−1.334	−1.948
	2PT(C)	−0.035	−0.699	−1.394	−2.016
	van der Hoef EOS	−0.152	−0.751	−1.429	−2.027

Self-diffusion coefficient D^*

		T^*			
ρ^*	Method[a]	1.8	1.4	1.1	0.9
0.05	$S(0)$	0.253	0.190	0.153	0.113
	Ruckenstein and Liu	0.248	0.201	0.160	0.131
0.40	$S(0)$	0.203	0.166	0.129	0.069
	Ruckenstein and Liu	0.197	0.159	0.128	0.105
0.70	$S(0)$	0.140	0.100	0.080	0.069
	Ruckenstein and Liu	0.136	0.106	0.083	0.067
0.85	$S(0)$	0.087	0.062	0.049	0.036
	Ruckenstein and Liu	0.089	0.065	0.047	0.036
1.10	$S(0)$	0.000	0.000	0.000	0.000
	Ruckenstein and Liu				

[a]MD, molecular dynamics results. MBWR EOS, modified Benedict–Webb–Rubin (MBWR) equation of Johnson *et al.* (Ref. 12); van der Hoef EOS, work of van der Hoef for the Lennard-Jones solid (Ref. 13). 1PT(Q): using harmonic approximation to DoS [Eq. (15)]. 2PT(C): DoS decomposition [Eq. (20)] with classical harmonic statistics [Eq. (16)] applied to the solid part. 2PT(Q) DoS decomposition [Eq. (20)] with quantum harmonic statistics [Eq. (15)] applied to the solid part. $S(0)$: Eq. (12). Ruckenstein and Liu: work of Ruckenstein and Liu (Ref. 14).

the recent work of van der Hoef[13] is chosen for the solid phase. These equations of state were parameterized to extensive, high quality MD or Monte Carlo (MC) simulations and can be taken as the best available theoretical values. We find that our results agree well with the literature values, with the exception of the two thermodynamically unstable points ($\rho^*=0.4$, $T^*=1.1$ and 0.9). For the $\rho^*=0.4$, $T^*=0.9$ unstable point we find that phase segregation has already occurred within the 240 ps simulation. For the three metastable states ($\rho^*=0.05$, $T^*=0.9$; $\rho^*=0.7$, $T^*=0.9$; and $\rho*$

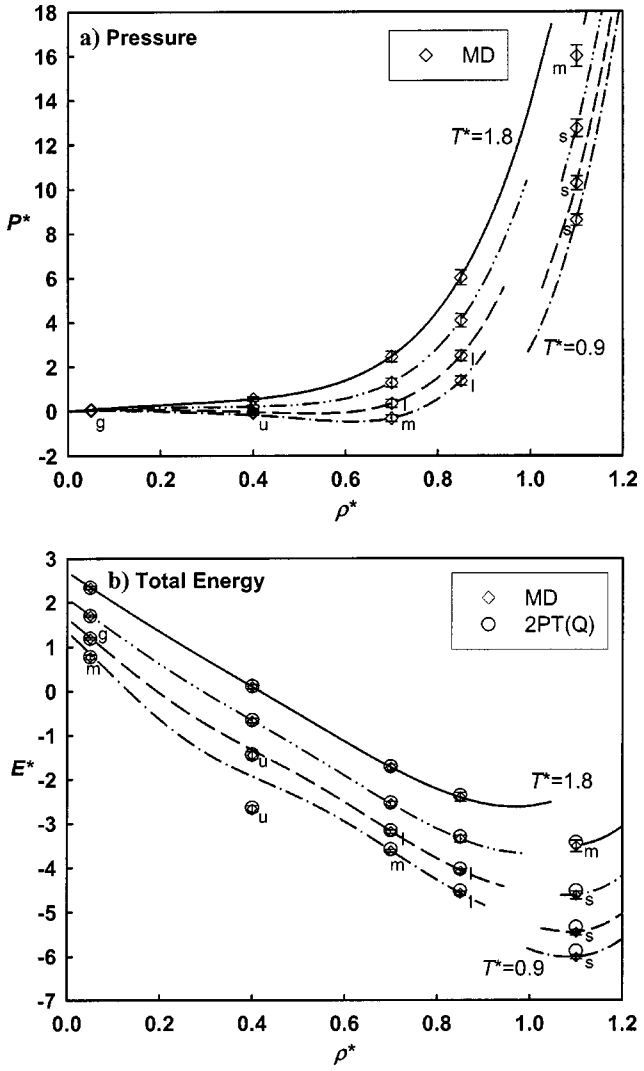

FIG. 4. The pressure (a) and energy (b) for Lennard-Jones systems. The curves are based on high quality equations of state (Refs. 12, 13) (solid, $T^*=1.8$; dot-dot-dashed, $T^*=1.4$; dashed, $T^*=1.1$; dot-dashed, $T^*=0.9$) the open diamonds are from our MD simulation, and the open circles are quantum corrected energies.

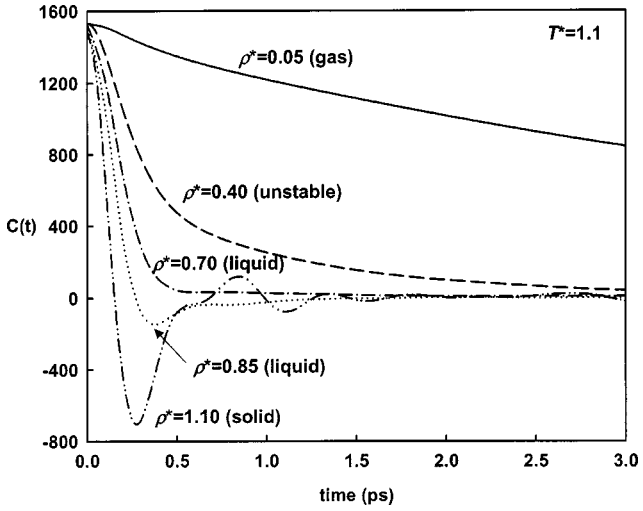

FIG. 5. The velocity autocorrelation (VAC) function for Lennard-Jones systems at $T^*=1.1$ and different densities: $\rho^*=0.05$ gas, $\rho^*=0.40$ unstable fluid, $\rho^*=0.70$ liquid, $\rho^*=0.85$ liquid, and $\rho^*=1.10$ crystal.

$=1.10$, $T^*=1.8$) no obvious phase segregation was observed and we find good agreement with the literature EOS.

The quantum effects in the LJ systems can be determined from the difference between the quantum statistical energy [2PT(Q) in Table III] and the MD energy. [Note that MD energy is equivalent to the classical energy, i.e., 2PT(C).] Quantum effects are in general small: essentially zero for LJ gases, about 1% in energy for the liquids, and 2% for the crystals studied here.

B. Velocity autocorrelation and density of state distribution

The velocity autocorrelation (VAC) as a function of time for LJ particles at temperature $T^*=1.1$ and different densities is shown in Fig. 5 and some of the corresponding vibrational density-of-state (DoS) distributions (representatives for gas, liquid, and solid) are presented in Fig. 6. For a gas, the VAC (Fig. 5, $\rho^*=0.05$) decays slowly and monotonically with time, resulting in a rapid and monotonic decay of $S(\upsilon)$ with frequency [Fig. 6(a)]. This is expected since the mean free path is much larger then the particle diameter for a LJ gas, leading to a collision probability that decreases rapidly with the number of collisions per unit time, proportional to the vibrational frequency. [For a true ideal gas, i.e., no collisions, the VAC would remain constant and the DoS would be a delta function at $\upsilon=0$.] For a crystal, the VAC (Fig. 5, $\rho^*=1.10$) oscillates around zero with the amplitudes decreasing with time. The oscillation of the VAC is a result of the incoherent vibration of the particles at their equilibrium positions. (For a single particle vibrating in a harmonic potential, the VAC is a cosine function and the DoS is a delta function.) The corresponding DoS has zero intensity at $\upsilon=0$ and increases gradually with frequency (as υ^2 according to Debye theory) [Fig. 6(c)]. The DoS of a LJ crystal has several peaks, reflecting the structured nature of crystals. For an amorphous solid (or glass), the distribution of $S(\upsilon)$ is expected to be smooth. The VAC (Fig. 5, $\rho^*=0.85$) and DoS [Fig. 6(b)] of a LJ liquid have characteristic of both gas phase and amorphous solids: The VAC oscillates around zero, and the $S(\upsilon)$ is finite at $\upsilon=0$ and goes through a maximum before it monotonically decays to zero. This special characteristic shape of the liquid state DoS provides the foundation of the DoS decomposition described in Sec. II D.

The decomposition of $S(\upsilon)$ based on the DoS distribution of a hard sphere gas is also presented in Fig. 6. In the low density and high temperature limit [Fig. 6(a)], the exponential decay of the velocity autocorrelation function for a hard-sphere gas results in a $S^g(\upsilon)$ closely resembling that of the true LJ gas. This is reasonable since the effects of the attractive part of LJ potential decays with increasing temperature. Consequently the repulsive part dominates at high temperatures and a LJ gas behaves much like a hard-sphere gas. In the case of a crystal [Fig. 6(c)], there is an insignificant amount of diffusive motion and $S^g(\upsilon)$ is essentially zero. For LJ liquids [Fig. 6(b)] the proposed decomposition scheme nicely partitions the overall $S(\upsilon)$ into a gaslike and a solidlike component.

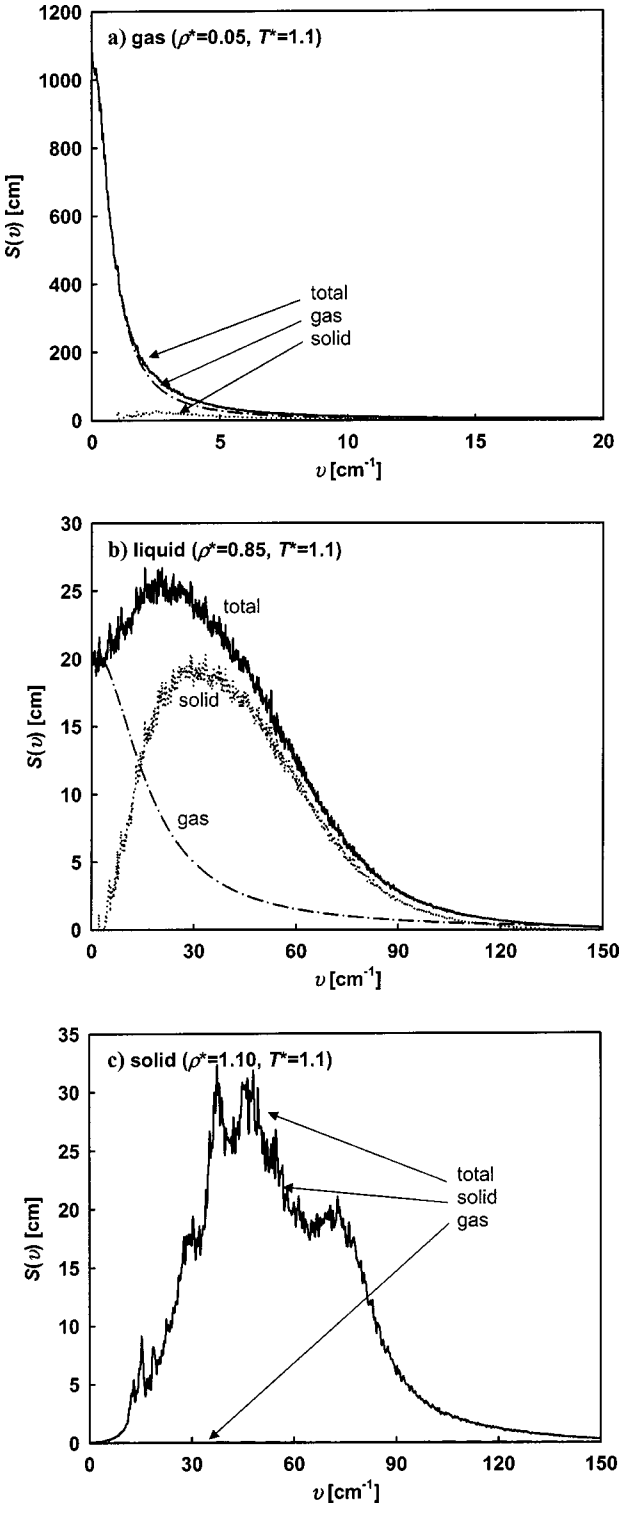

FIG. 6. The density of state distribution of LJ (a) gas ($\rho^*=0.05, T^*=1.1$), (b) liquid ($\rho^*=0.85, T^*=1.1$), and (c) fcc crystal ($\rho^*=1.10, T^*=1.1$). The total density of state distribution $S(\upsilon)$ is shown in black line, the gas component $S^g(\upsilon)$ determined with a hard sphere fluid in dot-dashed line, and the nondiffusive, solidlike component $S^s(\upsilon)$ in the dotted line.

The integrated area underneath each DoS distribution is equal to the number of degrees of freedom [Eq. (9)]. Therefore, the ratio of the areas from the diffusive modes and the overall system leads to the factor f, i.e.,

$$f=\frac{N^g}{N}=\frac{\int_0^\infty S^g(\upsilon)d\upsilon}{\int_0^\infty S(\upsilon)d\upsilon}. \tag{39}$$

From Fig. 6 and Table II the percentage of $S^g(\upsilon)$ increases with decreasing densities and increasing temperatures. In other words, there is more gaslike component in a system as the temperature increases and/or as the density decreases. Since the factor f increases monotonically with the normalized diffusivity Δ (Fig. 2), both parameters are a good measure of the ''fluidicity'' of a system. The proposed decomposition is not only reliable and stable, but is also physically meaningful.

C. Entropy and free energies: Fluidicity and quantum effects

The usefulness of the DoS decomposition method introduced here depends on the accuracy in calculating the thermodynamic properties. Figure 7(a) shows the entropy determined from the one-phase model with quantum statistics, 1PT(Q). For the crystalline phase ($\rho^*=1.10$) the entropy is calculated quite accurately, but for low-density fluids ($\rho^*=0.05,0.40$) it is overestimated while for high-density fluids ($\rho^*=0.70,0.85$) it is underestimated. In contrast, the 2PT method leads to a much more accurate entropy for all densities [Fig. 7(b)] regardless of the use of classical [2PT(C)] or quantum [2PT(Q)] statistics for the solid component.

Table III lists the numerical values of the calculated entropy from different methods. The problem with applying the harmonic approximation to the whole DoS, i.e., 1PT method, can be understood by examining the $S(\upsilon)$ in Fig. 6 and the weighting function in Fig. 8. At low densities, e.g., $T^*=1.1$ and $\rho^*=0.05$ (hard sphere packing fraction $fy=0.036$), most vibrational modes are located below $\upsilon=4$ cm^{-1} [Fig. 6(a)]. In this region, the HO weighting function (either quantum or classical) is much higher than that of the hard sphere (HS). Since in this condition the LJ gas behaves like a HS gas, the HO description overestimates the entropy.

The situation is somewhat different for liquids. The distribution of $S(\upsilon)$ is broadened: For example, at $T^*=1.1$ and $\rho^*=0.85$ ($fy=0.309$) the $S(\upsilon)$ extends to more than 100 cm^{-1} and has a maximum at around 20 cm^{-1} [Fig. 6(b)]. The HO description underestimates the entropy for this liquid case because the HO weighting is too small in the range between 4–100 cm^{-1}. This is also evidence for anharmonic effects in the liquid phase. The decomposition of the DoS, 2PT, allows us to separate the harmonic $S^s(\upsilon)$ and fluidic $S^g(\upsilon)$ components in the system to provide appropriate weights to each contributions. This leads to accurate values of entropy.

The quantum corrections to the entropy can be obtained by comparing the quantum and the classical entropies [open and closed circles in Fig. 7(b)]. Similar to the energy, the quantum effects are generally small and increase with increasing density or decreasing temperature. Roughly, quantum corrections in entropy are essentially zero for LJ gas, 0.5% for LJ liquid and, 1.8% for LJ crystals. The small quantum corrections in LJ systems can be understood as small differences between the entropy weighting functions of

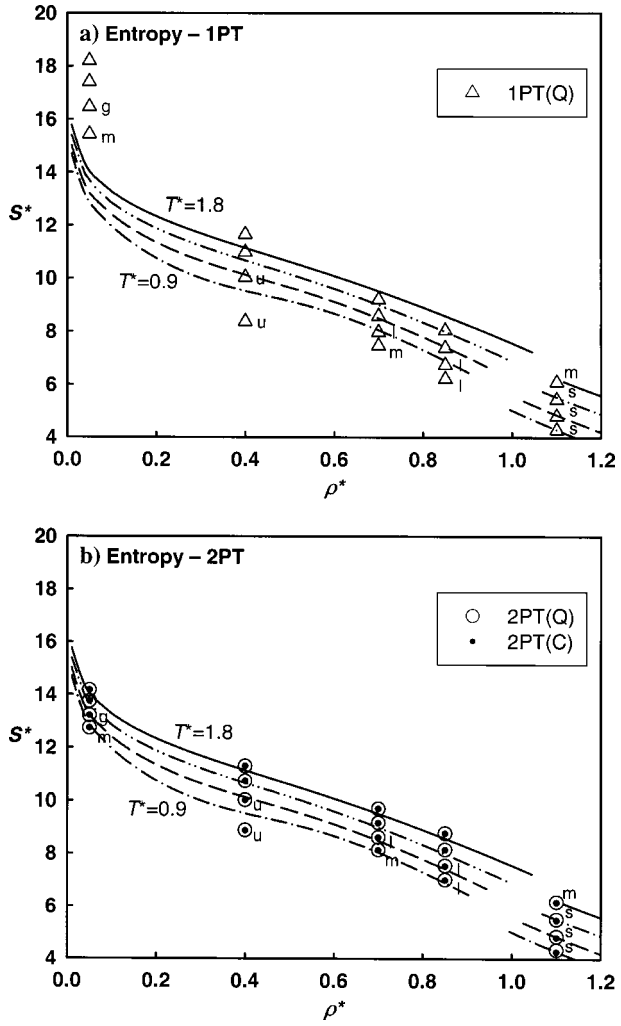

FIG. 7. Entropies determined from the density of state methods. (a) One-phase quantum 1PT(Q) model; (b) two-phase classical, 2PT(C) and quantum, 2PT(Q), models. The curves are based on equations of state predictions (Refs. 12, 13) (solid, $T^*=1.8$; dot-dot-dashed, $T^*=1.4$; dashed $T^*=1.1$; dot-dashed, $T^*=0.9$).

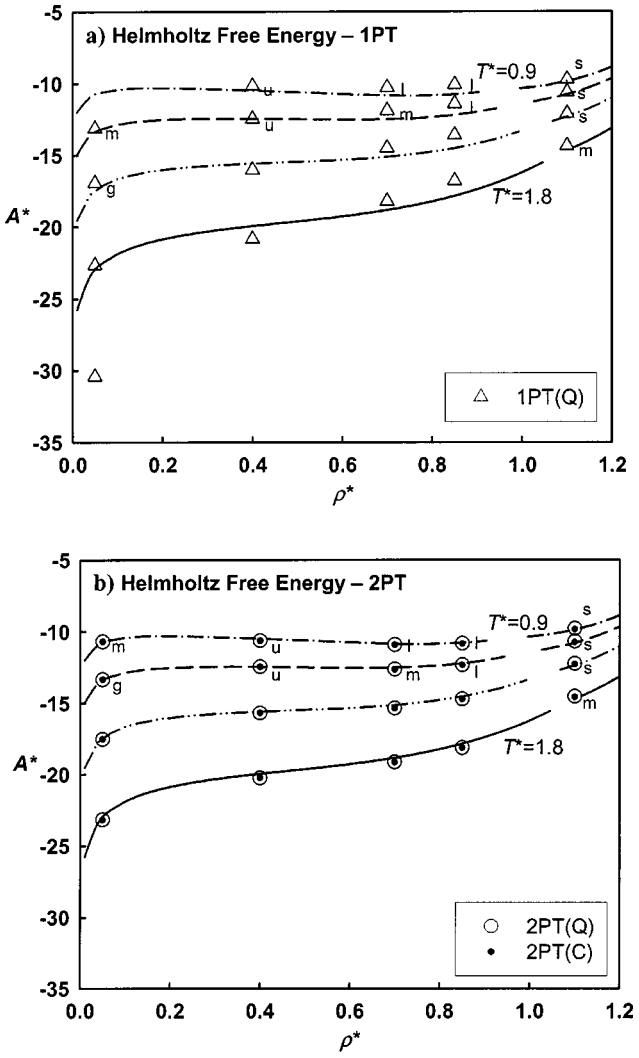

FIG. 9. Helmholtz free energies determined from the density of state methods. (a) One-phase quantum 1PT(Q) model, (b) two-phase classical, 2PT(C), and quantum, 2PT(Q), models. The curves are based on equations of state predictions (Refs. 12, 13) (solid, $T^*=1.8$; dot-dot-dashed, $T^*=1.4$; dashed, $T^*=1.1$; dot-dashed, $T^*=0.9$).

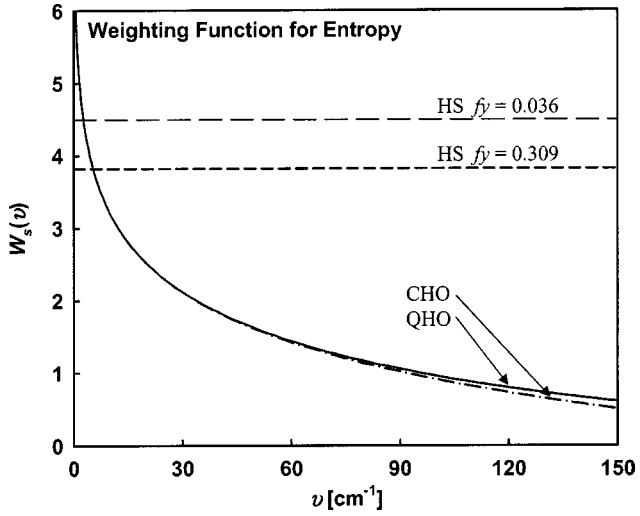

FIG. 8. Comparison of the entropy weighting function for a classical harmonic oscillator (HO), a quantum harmonic oscillator (QHO), and a hard sphere (HS) fluid at $T^*=1.1$ with gas phase packing fraction $fy=0.036$ and $T^*=1.1$ with $fy=0.309$.

quantum and classical HO (Fig. 8) within the range of $\upsilon < 150\ \mathrm{cm}^{-1}$. For molecular system with strong interactions, e.g., covalent and hydrogen bonds, quantum effects will be more significant.

Figures 9 and 10 and Table III compare the calculated Helmholtz ($A^*=E^*-T^*S^*$) and Gibbs ($G^*=A^*+P^*/\rho^*$) free energies. Due to the inaccuracy in determining the entropy, the 1PT method underestimates the free energies at low densities and overestimates them at high densities. The 2PT method overall gives very good agreement with the EOS values. It is interesting to note that the calculated properties in the metastable regime also agree well with EOS. Consequently the 2PT method should be useful for studying the thermodynamic driving forces for nucleation and the viscosity of metallic glasses. It should also be useful for dynamical systems involving time scales and transport coefficients, including in phase transitions, that may not be accessible to Monte Carlo methods.

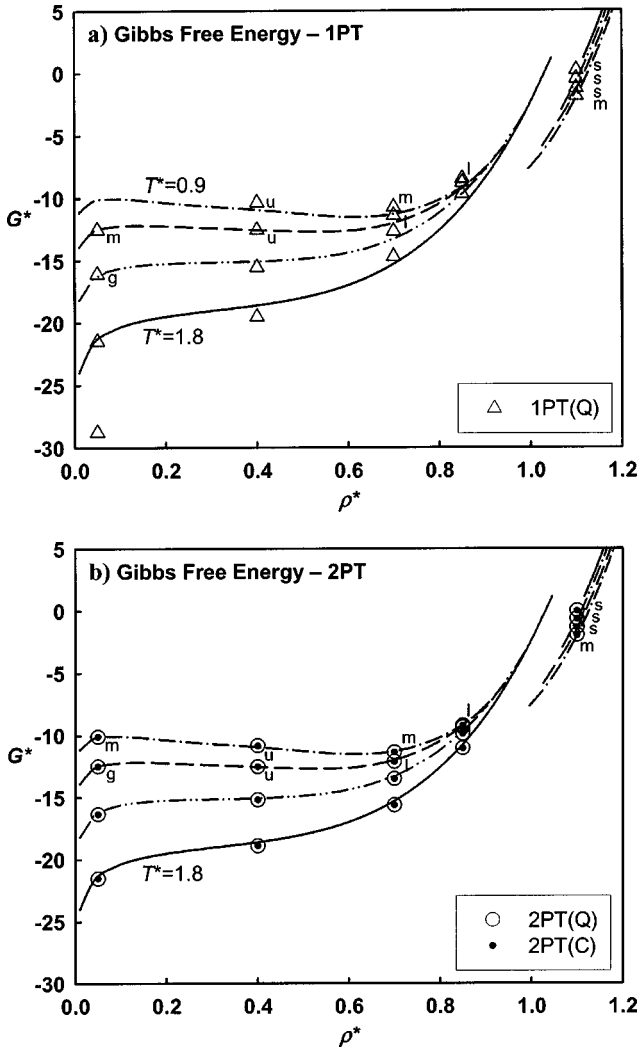

FIG. 10. Gibbs free energies determined from the density of state methods. (a) One-phase quantum 1PT(Q) model and (b) two-phase classical, 2PT(C), and quantum, 2PT(Q), models. The curves are based on equations of state predictions (Refs. 12, 13) (solid, $T^*=1.8$; dot-dot-dashed, $T^*=1.4$; dashed, $T^*=1.1$; dot-dashed, $T^*=0.9$).

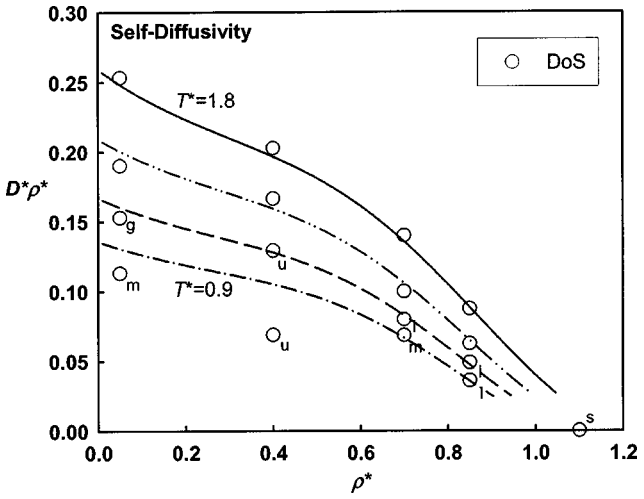

FIG. 11. Reduced diffusivity (multiplied by reduced density) determined from the zero frequency value of the DoS [Eq. (12)]. The curves are based on the work of Ruckenstein and Liu (Ref. 14) (solid, $T^*=1.8$; dot-dot-dashed, $T^*=1.4$; dashed, $T^*=1.1$; dot-dashed, $T^*=0.9$).

D. Self-diffusion coefficient

We compare in Fig. 11 and Table III the calculated self-diffusion coefficients with a model recently developed by Ruckenstein and Liu.[14] Their model was fitted to various simulations results at conditions ranging from $T^*=0.72$ to 10.0 and $\rho^*=0.00$ to 1.12, and is considered by us to give good ''averaged'' literature values. We find that there is an excellent agreement with the literature values. Thus the use of $S(0)$ gives very reliable values for self-diffusion coefficients in liquids. Our calculated values tend to deviate from Ruckenstein and Liu's values for dilute gases at low temperature, as their model may have larger relative errors at low temperatures.[14]

E. Convergence efficiency

A particularly attractive feature of the 2PT model developed here is that it is quite efficient for obtaining converged thermodynamic properties, especially for liquids. Figure 12 compares the entropy values calculated from MD trajectories of different lengths (from 2.5 ps to 2.5 ns) for a LJ gas ($\rho^*=0.05, T^*=1.8$) and a liquid ($\rho^*=0.85, T^*=0.9$). The numerical values are listed in Table IV. The entropy for the gas phase system converges to within 0.2% with 2500 MD steps (20 ps) and for the liquid phases converges to within 1.5% with 2500 MD steps (20 ps). Thus the 2PT method is much more computationally efficient than test particle (TP) or thermodynamic integration (TI) techniques, where millions of samplings are usually necessary to obtain good statistics. The reason for the efficiency of 2PT is the very efficient use of trajectory information. In 2PT, the evolution of velocities from *all* the particles are used to establish the DoS, which is later used to determine the thermodynamic properties. In contrast, other methods (TP, TI, etc.) usually use only *one* probe particle to build up the statistics at each simulation step. Therefore, we expect the 2PT method to be N times (N being the number of particles in the system) more efficient than other methods. This makes 2PT an attractive method to study thermodynamic properties for complex systems.

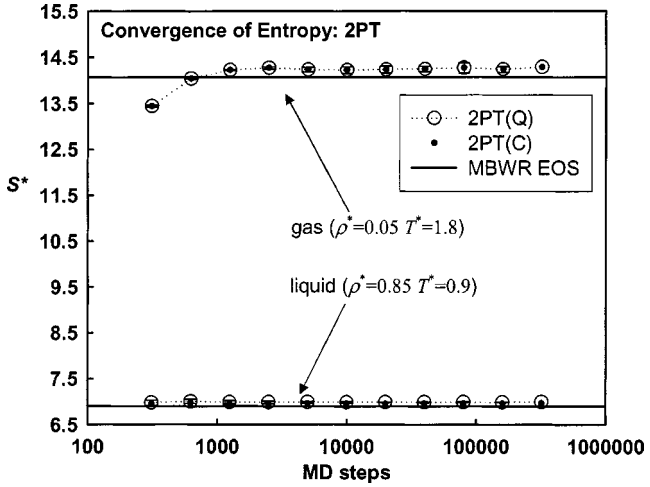

FIG. 12. Calculated entropy from the 2PT method with trajectory of different lengths for a LJ gas ($\rho^*=0.05, T^*=1.8$) and liquid ($\rho^*=0.85, T^*=0.9$). One MD step corresponds to 8 fs (10^{-15} s).

TABLE IV. Convergence of the 2PT method for LJ gas ($\rho^*=0.05$, $T^*=1.8$) and liquid ($\rho^*=0.85$, $T^*=0.9$).

MD steps	313	625	1250	2500	5000	10000	20000	40000	80000	160000	320000
time (ps)	2.5	5	10	20	40	80	160	320	640	1280	2560
No. samples	1024	512	256	128	64	32	16	8	4	2	1
					$\rho^*=0.05$, $T^*=1.8$ (gas)						
2PT(Q)	13.444	14.040	14.224	14.274	14.234	14.225	14.237	14.248	14.270	14.242	14.286
dev[a]	0.020	0.015	0.015	0.025	0.050	0.072	0.080	0.059	0.113	0.067	
2PT(C)	13.442	14.040	14.224	14.274	14.234	14.225	14.237	14.248	14.270	14.242	14.286
dev[a]	0.020	0.015	0.015	0.025	0.050	0.072	0.080	0.059	0.113	0.067	
MBWR EOS[b]						14.071					
					$\rho^*=0.85$, $T^*=0.9$ (liquid)						
2PT(Q)	6.980	7.004	6.989	6.989	6.991	6.989	6.987	6.991	6.992	6.991	6.995
dev[a]	0.056	0.046	0.038	0.028	0.019	0.016	0.009	0.008	0.006	0.004	
2PT(C)	6.946	6.972	6.957	6.958	6.960	6.958	6.957	6.960	6.961	6.960	6.965
dev[a]	0.057	0.046	0.038	0.028	0.020	0.017	0.009	0.008	0.006	0.004	
MBWR EOS[b]						6.899					

[a]Standard deviation.
[b]Modified Benedict–Webb–Rubin (MBWR) equation of Johnson *et al.* (Ref. 12).

V. CONCLUSIONS AND OUTLOOK

This work develops the 2 phase thermodynamics (2PT) approach for calculating the thermodynamic properties of fluids from single molecular dynamics simulation trajectories. The 2PT method makes use of the vibrational density of states extracted from MD trajectories. Other approaches have been suggested for determining thermodynamic properties from the MD derived vibrational density of states or from the normal modes of the system. The 2PT method is unique in that explicit consideration of fluidicity effects at low frequencies is made together with quantum corrections. The 2PT DoS decomposition scheme provides an analytic separation of the diffusive, fluidic component in the DoS. This allows a separate treatment of harmonic, fluidic, and quantum effects, resulting in an accurate description of the thermodynamic properties.

Attractive features of the 2PT method for calculating entropy and free energy include:

(1) Thermodynamic and transport properties are determined simultaneously.
(2) Only short simulation times (20 ps) are needed to obtain high accuracy. For a system with N particles, we expect 2PT to be N times faster than methods such as particle insertion and thermodynamic integration.
(3) The efficiency of 2PT does *not* deteriorate with increasing density (a severe limitation in most other techniques).
(4) The properties are obtained under fully equilibrated conditions (no perturbation in the simulation itself).
(5) Zero point energy and corrections for quantum effects are included.
(6) 2PT can be used to determine the properties in metastable and unstable regimes.
(7) 2PT could also be used for nonequilibrium systems to estimate effects of transient effects, reaction, and phase transitions, since it is only necessary to have stabilities over time scales of ~20 ps.

In this paper we validated the 2PT method for pure LJ fluids, but the method applies with no modification to general force fields. We expect that the 2PT method provides the necessary information for calculating such other transport properties as viscosity and thermal conductivity.

ACKNOWLEDGMENTS

The authors would like to thank Dr. Tahir Çağin, Dr. Seung Soon Jang, Dr. Prabal Maiti, Dr. Valeria Molinero, and Peng Xu for many useful discussions. This research was partially supported by the NSF (CHE 99-85774, CTS-0132002) and NIH (1R01-GM62523-01). The facilities of the MSC used in this research are also supported by grants from DOE (ASCI and FETL), ARO (MURI and DURIP), ONR (MURI and DURIP), IBM-SUR, General Motors, ChevronTexaco, Seiko-Epson, Asahi Kasai, Beckman Institute, and Toray.

[1] D. Frenkel and B. Smit, *Understanding Molecular Simulation From Algorithms to Applications* (Academic, New York, 2002).
[2] A. A. McQuarrie, *Statistical Mechanics* (Harper & Row, New York, 1976).
[3] P. H. Berens, D. H. J. Mackay, G. M. White, and K. R. Wilson, J. Chem. Phys. **79**, 2375 (1983).
[4] M. Karplus and J. N. Kushick, Macromolecules **14**, 325 (1981).
[5] J. Schlitter, Chem. Phys. Lett. **215**, 617 (1993).
[6] I. Andricioaei and M. Karplus, J. Chem. Phys. **115**, 6289 (2001).
[7] H. Schäfer, A. E. Mark, and W. F. van Gunsteren, J. Chem. Phys. **113**, 7809 (2000).
[8] H. Schäfer, X. Daura, A. E. Mark, and W. F. van Gunsteren, Proteins: Struct., Funct., Genet. **43**, 45 (2001).
[9] N. F. Carnahan and K. E. Starling, J. Chem. Phys. **53**, 600 (1970).
[10] CERIUS2 (Molecular Simulations Inc., San Diego, 1999).
[11] N. Karasawa and W. A. Goddard, J. Phys. Chem. **93**, 7320 (1989).
[12] J. K. Johnson, J. A. Zollweg, and K. E. Gubbins, Mol. Phys. **78**, 591 (1993).
[13] M. A. van der Hoef, J. Chem. Phys. **113**, 8142 (2000).
[14] E. Ruckenstein and H. Q. Liu, Ind. Eng. Chem. Res. **36**, 3927 (1997).